Freezing and Melting of Nitrogen, Carbon Monoxide, and Krypton in a Single Cylindrical Pore

Kunimitsu Morishige* and Keizi Kawano

Department of Chemistry, Okayama University of Science, 1-1 Ridai-cho, Okayama 700-0005, Japan

Received: November 5, 1999; In Final Form: January 11, 2000

To study the freezing/melting behavior of a confined N_2, CO, and Kr, we performed X-ray diffraction measurements of N_2, CO, and Kr confined inside the cylindrical pores of five kinds of siliceous MCM-41 with different pore radii ($R = 1.45-2.9$ nm) as a function of temperature. Freezing and melting of these three molecules were almost reversible for all the MCM-41 samples used here. Freezing of the CO confined to the mesopores resulted in the appearance of the orientationally ordered α phase, whereas the N_2 solidified into the orientationally disordered phase analogous to the bulk β phase. The solid Kr confined to the mesopores contains a considerable amount of random stacking faults. The freezing-point depressions of N_2 and CO relative to the bulk melting point were nearly the same and were slightly larger than that of Kr. Upon cooling, both molecular liquids of N_2 and CO confined to the cylindrical mesopores of $R = 2.1$ nm vitrify, whereas liquid Kr crystallizes within the mesopores of $R = 1.8$ nm and vitrifies within the mesopores of $R = 1.45$ nm. The mechanism of vitrification of a confined liquid upon cooling is considered.

I. Introduction

There is considerable current interest in the freezing and melting behavior of materials confined in porous media, especially in porous silicas. A wide variety of materials such as hydrogen,[1,2] deuterium,[3,4] helium,[5] neon,[2] argon,[2] krypton,[6] oxygen,[2,4,7] nitrogen,[6] methane,[8] carbon dioxide,[9] water,[6,10−12] methyl chloride,[13] cyclohexane,[14,15] succinonitrile,[16] 2,4,6-trinitrotoluene,[17] sodium nitrate,[18] indium,[19] gallium,[20] and mercury[21,22] have been explored. It is well known that their freezing and melting temperature is always depressed compared with the bulk and a large hysteresis effect is often observed between freezing and melting. The structure of the frozen solid phase within pores is sometimes different from that of the bulk and ultimately becomes amorphous in smaller pores.

Despite progress in our understanding of the freezing/melting behavior of confined materials, however, there are many fundamental questions remaining to be answered. For example, the effects of finite size and surface interactions on the structure of a confined solid are still unclear. The origin of the hysteresis between freezing and melting is controversial. In our previous reports[12,13] we have proposed that the hysteresis arises from genuine supercooling, namely the presence of a kinetic barrier to crystallization, and a small amount of gap between the normal freezing point and the glass transition temperature for a given material would easily lead to the freezing of a supercooled state, that is, the appearance of a glassy state, owing to a large freezing-point depression due to the Gibbs−Thomson effect.

Recent studies[6,8,10,12,13,23,24] show that MCM-41 can be regarded as the most suitable model adsorbent currently available for mesopores. The pores are of cylindrical-like nature, arranged parallel in a honeycomb-type lattice, and their dimensions can be tailored in the range 2−10 nm or more. The absence of pore channel intersections in MCM-41 guarantees that pore-networking effects are negligibly small. Neutron diffraction studies[6] on an MCM-41 sample with pore radius of 2 nm have shown that on cooling, Kr solidifies into a crystalline phase, whereas N_2 does not crystallize. X-ray diffraction studies[25] on conventional mesoporous materials have shown that the frozen phase of Kr confined to the pores declines in crystallinity with decreasing pore size and ultimately becomes amorphous for the pores of radius 1.1 nm. On the other hand, upon solidification, water crystallizes even within the MCM-41 sample with small pore radius of 1.2 nm.[12] Therefore, it is interesting to understand why a glassy state easily appears for some molecules confined to the mesopores.

The purpose of the present study is to address the above-mentioned problem by examining the freezing and melting behavior, as well as the structures of the frozen solid, of N_2, CO, and Kr confined in MCM-41 adsorbents with well-defined pore radii by means of X-ray diffraction. The CO and N_2 molecules form an orientationally ordered α phase at low temperature and an orientationally disordered β phase at high temperature, below their triple points.[26,27] Although both molecules have many similarities in their physical properties, the phase-transition temperatures between the α and β phases differ significantly. This arises mainly from the difference in magnitude between the quadrupole moments of both molecules. On the other hand, the difference in melting point is rather small. The Kr molecule has no electric moment. Therefore, we can explore the effects of the quadrupole moment on the structure and phase transitions of a confined phase by comparing the phase transition behavior of these molecules confined in the MCM-41.

II. Experimental Section

Sample preparations and characterization have been described in a previous paper.[12] Five kinds of MCM-41 adsorbents with pore radii (R) of 1.45, 1.8, 2.1, 2.5, and 2.9 nm were used in the present experiments.

The experimental apparatus of X-ray diffraction for freezing/melting measurements has been also described in detail else-

* Author for correspondence. Fax: 086-254-2891; e-mail: morishi@chem.ous.ac.jp.

10.1021/jp993919h CCC: $19.00
Published on Web 03/10/2000

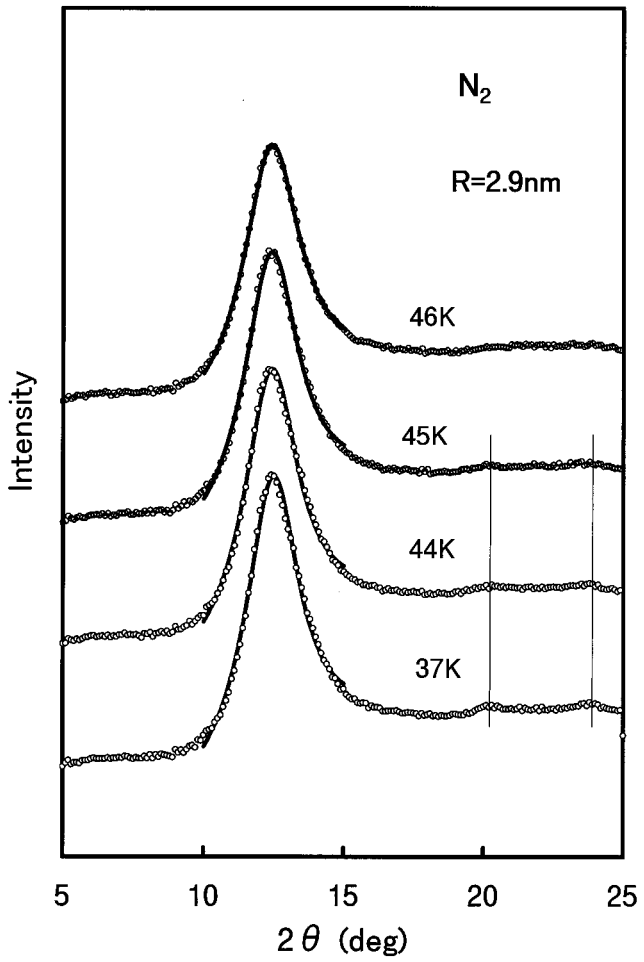

Figure 1. Change of X-ray diffraction pattern of N_2 confined to the cylindrical mesopores of $R = 2.9$ nm upon cooling. Solid lines are Lorentzian fits to the data.

where.[28] The measurements were carried out with MoKα radiation in a symmetrical transmission geometry. An MCM-41 self-supporting disk (~0.02 g) of 12 mm diameter was attached to a cold head of a He closed-cycle refrigerator. After prolonged evacuation at room temperature, the substrate was cooled and then the background spectra were measured. Adsorption isotherms of N_2, CO, and Kr on MCM-41 inside the X-ray cryostat were measured at 55, 55, and 90 K, respectively. In X-ray measurements, the adsorbed amounts were kept slightly below the saturation to avoid contamination in diffraction pattern from the bulk phase formed outside the mesopores. The substrate was then cooled to a desired temperature, and the spectrum was remeasured. After correction for attenuation due to substrate and adsorbed gas, the diffraction pattern of a confined phase was obtained by subtraction of data for charged and empty substrates.

III. Results

All the adsorption isotherms of N_2, CO, and Kr on MCM-41 were of type IV. The step due to capillary condensation shifted into higher pressure with increasing R.

Figure 1 shows some of the diffraction patterns from the N_2 confined to the cylindrical pores of radius 2.9 nm when the temperature was successively lowered. On cooling, one obtains still pure liquid scattering at 46 K, well below the bulk melting point of 63.15 K.[29] As the temperature is further lowered through 45 K, there is a rather abrupt change in the diffraction pattern from liquid to solid form. The latter is characterized by the

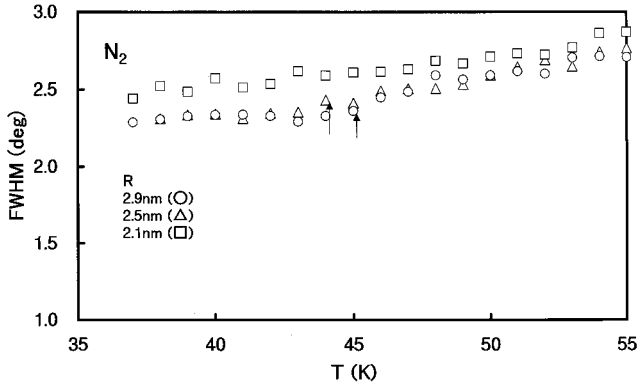

Figure 2. Peak width (fwhm) as a function of temperature for N_2 confined to the cylindrical mesopores of MCM-41. To improve clarity, only the data upon cooling are given. Vertical arrows denote the freezing points.

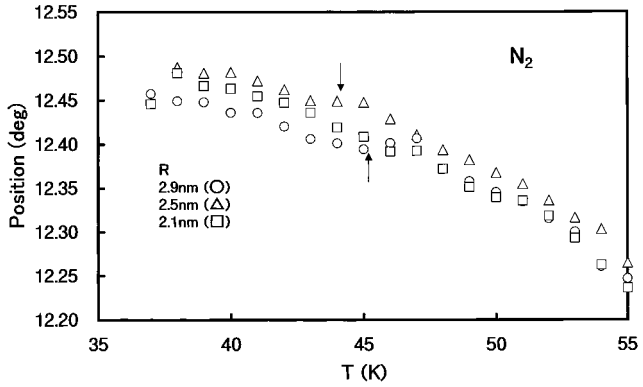

Figure 3. Peak position as a function of temperature for N_2 confined to the cylindrical mesopores of MCM-41. To improve clarity, only the data upon cooling are given. Vertical arrows denote the freezing points.

appearance of two small peaks at $2\theta = 20.2$ and 23.8°. For the N_2 confined to the mesopores of $R = 2.5$ nm, similar transformation of the diffraction pattern was observed, although the solidification temperature was slightly lowered. On the other hand, the freezing behavior changed significantly for the N_2 confined to the mesopores of $R = 2.1$ nm. The diffraction pattern did not give any evidence for the formation of a crystalline solid even at the lowest temperature (37 K). Freezing and melting were almost reversible for all the MCM-41 samples used here.

To obtain accurate peak parameters, the observed peak profile was fitted to a Lorentzian line shape with a linearly changing background in a limited 2θ range. The solid lines in Figure 1 are fits to a Lorentzian line shape. Figures 2 and 3 show the peak widths [full width at half-maximum (fwhm)] and positions, respectively, obtained from Lorentzian fits to the main peaks as a function of temperature for the N_2 confined to the cylindrical pores of MCM-41. For the N_2 confined to the mesopores of $R = 2.5$ and 2.9 nm, the peak width decreased gradually with decreasing temperature up to their freezing points. On the other hand, the peak width for the N_2 within the mesopores of $R = 2.1$ nm decreased almost linearly with decreasing temperature in the whole range of temperature examined. For the N_2 confined to the mesopores of $R = 2.9$ nm, the temperature dependence of the peak position showed an anomaly near its freezing point; upon solidification the peak position shifted slightly into lower scattering angle. Solidification results in shrinkage of most materials, usually leading to a shift of the peak position into higher scattering angle. It was impossible to find any features ascribable to freezing on the relation between the peak position and temperature for the N_2

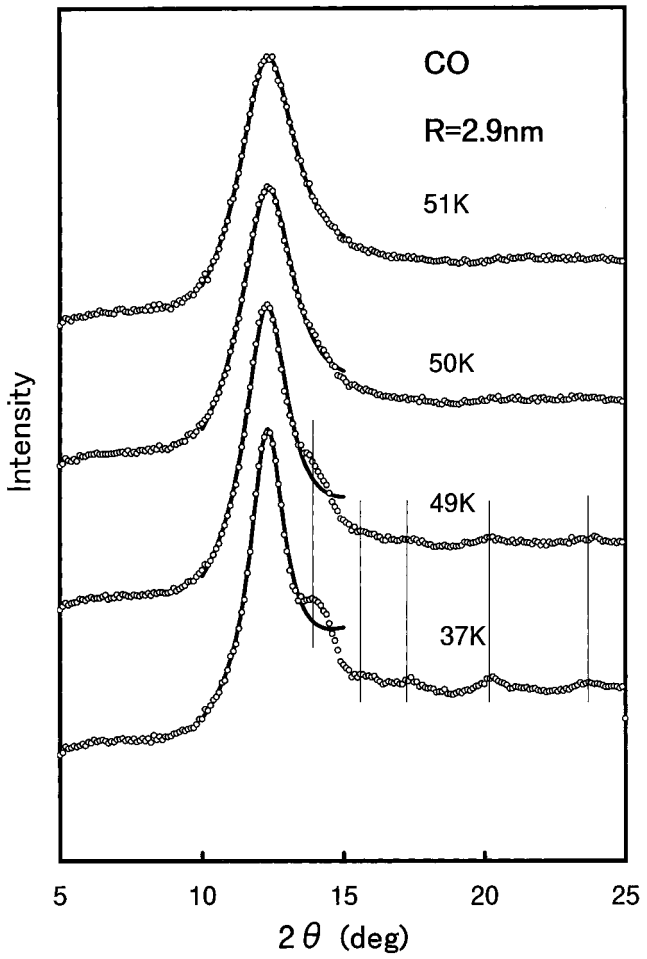

Figure 4. Change of X-ray diffraction pattern of CO confined to the cylindrical mesopores of $R = 2.9$ nm upon cooling. Solid lines are Lorentzian fits to the data.

confined to the mesopores of $R = 2.1$ nm. Therefore, it is uncertain whether the N_2 phase confined to the mesopores of $R = 2.1$ nm is a solid at 37 K, the lowest temperature examined here.

Figure 4 shows some of the diffraction patterns from the CO confined to the mesopores of $R = 2.9$ nm when the temperature was successively lowered. One obtains still pure liquid scattering at 50 K, well below the bulk melting point of 68.10 K.[29] As the temperature is lowered through 49 K, there is a rather abrupt change in the diffraction pattern from liquid to solid form. The latter is characterized by the appearance of five small peaks at $2\theta = 14.1$, 15.9, 17.4, 20.3, and 23.7°. For the CO confined to the mesopores of $R = 2.5$ nm, similar transformation of the diffraction pattern was observed, although the solidification temperature was further lowered by ~1 K. The freezing behavior of the CO confined to the pores of $R = 2.1$ nm changed significantly. The diffraction pattern did not give any evidence for the formation of a crystalline solid even at the lowest temperature (37 K). Freezing and melting were almost reversible for all the MCM-41 samples used here. Figures 5 and 6 show the peak widths and positions, respectively, obtained from Lorentzian fits to the main peaks as a function of temperature for the CO confined to the pores of MCM-41. For the CO confined to the mesopores of $R = 2.9$ nm, the peak width decreased abruptly on freezing at 49 K, being in a good agreement with the appearance of the crystalline peaks in the diffraction pattern. Similarly, the peak width for the CO confined to the mesopores of $R = 2.5$ nm decreased remarkably on

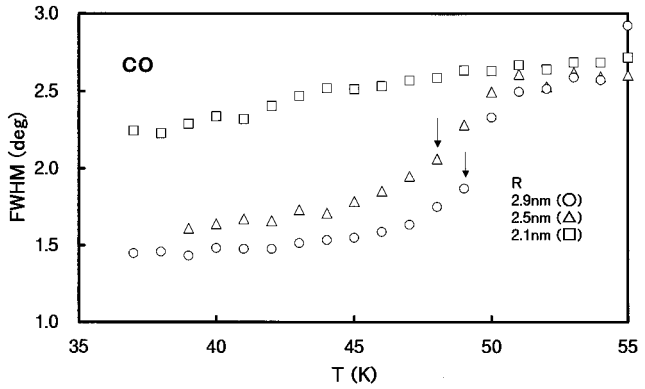

Figure 5. Peak width (fwhm) as a function of temperature for CO confined to the cylindrical mesopores of MCM-41. To improve clarity, only the data upon cooling are given. Vertical arrows denote the freezing points.

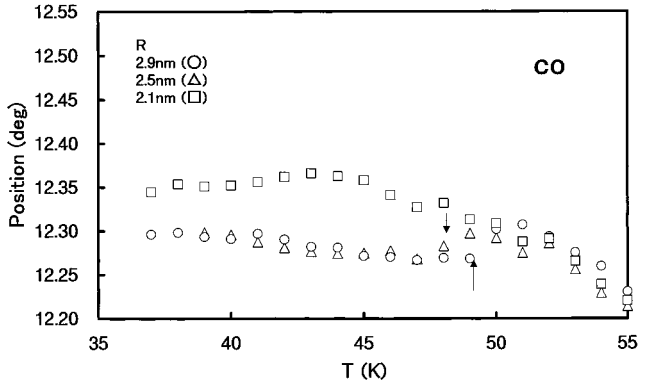

Figure 6. Peak position as a function of temperature for CO confined to the cylindrical mesopores of MCM-41. To improve clarity, only the data upon cooling are given. Vertical arrows denote the freezing points.

freezing at 48 K. For the CO confined to the mesopores of $R = 2.1$ nm, the peak width decreased slightly up to 42 K with decreasing temperature, although its variation was very small compared with those for larger pores. For the CO confined to both the mesopores of $R = 2.9$ and 2.5 nm, the temperature dependence of the peak position showed anomalies similar to that observed for the N_2 confined to the pores of $R = 2.9$ nm near their freezing points. For the CO confined to the mesopores of $R = 2.1$ nm, the temperature dependence of the peak position reversed around 44 K. This suggests the appearance of a glassy state. Both the CO and N_2 phases confined within MCM-41 did not show any evidence for the appearance of a solid−solid phase transition in the temperature region examined here.

Figure 7 shows some of the diffraction patterns from the Kr confined to the mesopores of $R = 2.9$ nm when the temperature was successively lowered. As the temperature is lowered through 88 K, well below the bulk melting point of 115.95 K,[29] there is a rather abrupt change in the diffraction pattern from liquid to solid form. The latter is characterized by the splitting of a broad peak centered at $2\theta = 22.5°$ into two sharp peaks at $2\theta = 20.3$ and 23.6°. Similar transformation of the diffraction pattern was observed for the Kr confined to the mesopores of $R = 2.5$, 2.1, and 1.8 nm, whereas for the Kr confined to the mesopores of $R = 1.45$ nm the diffraction pattern did not give any evidence for the formation of a crystalline solid in the temperature range 90−60 K. When the temperature was further lowered below 60 K, desorption of the Kr confined to the mesopores of MCM-41 occurred in the temperature range 60−40 K. The amount of desorption increased with increasing pore size. When the temperature was then increased, adsorption of Kr inside the

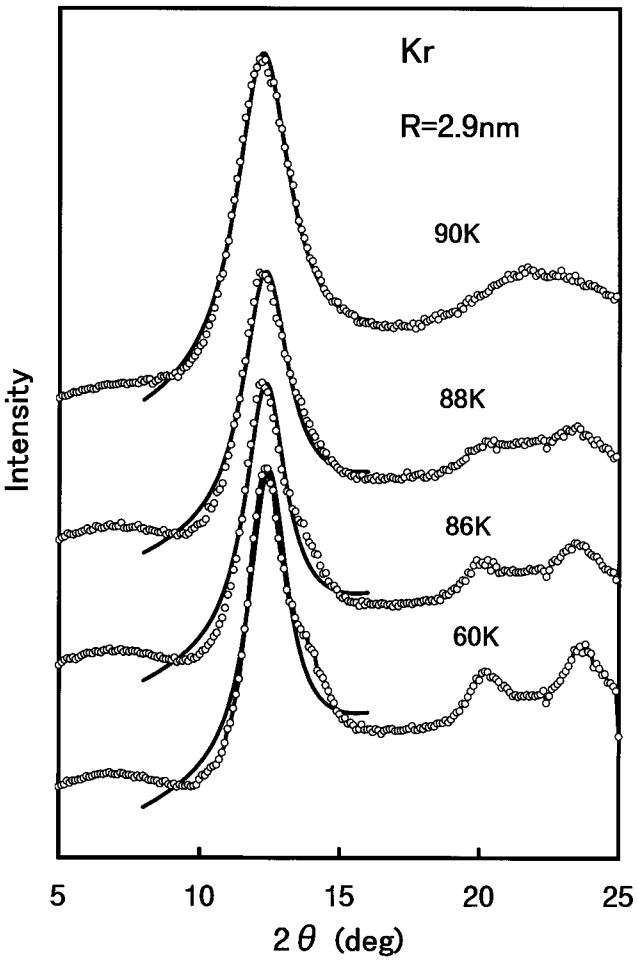

Figure 7. Change of X-ray diffraction pattern of Kr confined to the cylindrical mesopores of $R = 2.9$ nm upon cooling. Solid lines are Lorentzian fits to the data.

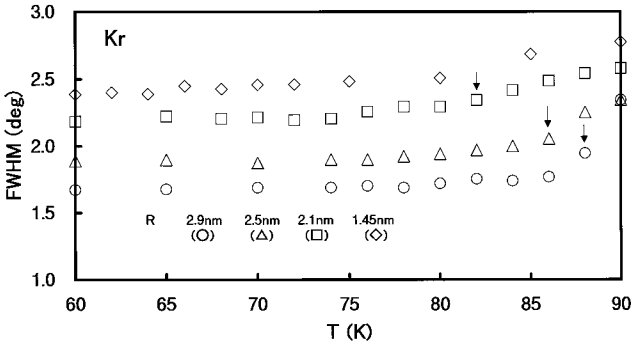

Figure 8. Peak width (fwhm) as a function of temperature for Kr confined to the cylindrical mesopores of MCM-41. To improve clarity, only the data upon cooling are given and also the data for $R = 1.8$ nm are deleted. Vertical arrows denote the freezing points.

mesopores occurred in the temperature range 50−70 K. Freezing and melting, however, were almost reversible for all the MCM-41 samples. Figures 8 and 9 show the peak widths and positions, respectively, as a function of temperature. For the Kr confined to the mesopores of $R = 2.9$ and 2.5 nm, the peak position shifted into higher scattering angle upon solidification as expected from shrinkage of the phase. The shift of the peak position upon solidification was negligible for the Kr confined to the mesopores of $R = 2.1$ and 1.8 nm. The amount of supercooling increases with decreasing pore-size and the difference in density between a supercooled liquid and a solid decreases with decreasing temperature. This partly explains the

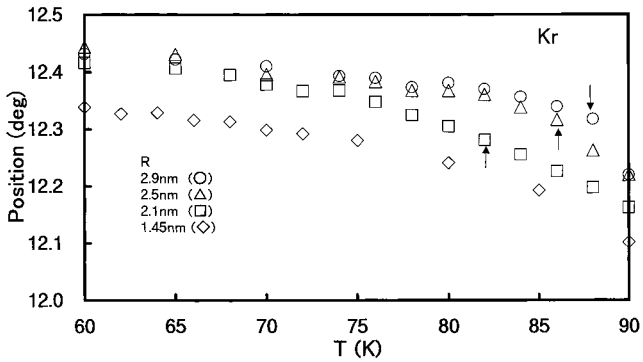

Figure 9. Peak position as a function of temperature for Kr confined to the cylindrical mesopores of MCM-41. To improve clarity, only the data upon cooling are given and also the data for $R = 1.8$ nm are deleted. Vertical arrows denote the freezing points.

TABLE 1: Freezing Temperatures (K) of N_2, CO, and Kr Confined in MCM-41

R (nm)	N_2	CO	Kr
2.9	45	49	88
2.5	44	48	86
2.1			82
1.8			76

fact that the shift of the peak position upon solidification becomes smaller with decreasing pore size. Table 1 summarizes the freezing temperatures of the N_2, CO, and Kr confined in MCM-41.

IV. Discussion

The CO and N_2 molecules have similarities in many physical characteristics such as size, molecular mass, quadrupole moment, thermodynamic properties, total X-ray scattering factor, and so on.[30] The quadrupole moment has a major role in determining the low-temperature structure and phase transitions. The bulk phases of N_2 and CO also have many similarities.[26,27] At low temperature both molecules have an α phase in which the orientation of the molecular axes are dominated by the quadrupolar interactions between the molecules. The center of X-ray scattering of each molecule in the α phases is located close to the sites of a face-centered cubic (fcc) lattice. Four molecules are in each unit cell, and each of these four molecules has a unique molecular direction in the unit cell. At high temperature both CO and N_2 have an orientationally disordered β phase in which the molecules are precessing about the (111) directions. Both the β phases form hexagonal close-packed (hcp) structures. Because the quadrupole moment of a CO molecule is about 30% bigger than that of N_2, we expect the orientational ordering transition temperature between the α and β phases of CO (61.53 K) to be higher than that of N_2 (35.62 K).[29] The melting point of CO (68.10 K) is slightly higher than that of N_2 (63.15 K).[29] Enthalpy changes of melting and $\alpha-\beta$ transition of CO are 0.84 and 0.63 kJ/mol, respectively, whereas enthalpy changes of melting and $\alpha-\beta$ transition of N_2 are 0.72 and 0.23 kJ/mol, respectively.[29] The bulk solid of Kr consists of an fcc lattice and the size is similar to those of the CO and N_2 molecules. The melting of Kr (115.95 K) is characterized by an enthalpy change of 1.64 kJ/mol.[29]

A. Structure of Confined Solid. Figure 10 shows the X-ray diffraction patterns of the frozen Kr phase confined to the cylindrical mesopores of MCM-41 as a function of pore size at 60 K. The diffraction pattern for $R = 2.5$ nm is crystalline, whereas that for $R = 1.45$ nm is amorphous. The diffraction pattern for $R = 2.1$ nm seems to be a superposition of crystalline

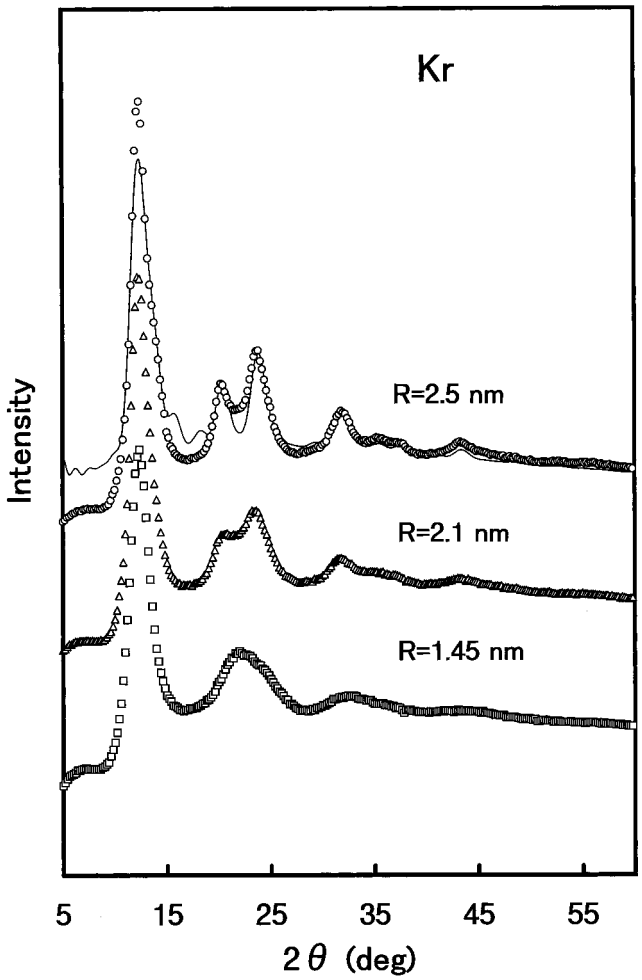

Figure 10. 10. X-ray diffraction patterns of Kr confined within MCM-41 as a function of pore size at 60 K. Solid line denotes the simulated pattern of the spheres of radius 1.6 nm with stacking sequence ABCBCABCA.

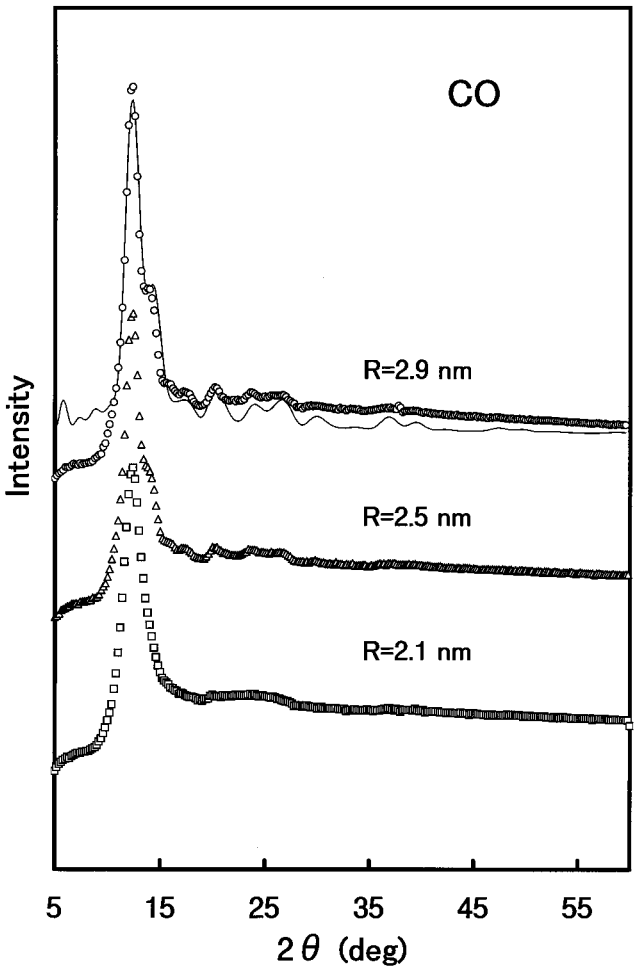

Figure 11. X-ray diffraction patterns of CO confined within MCM-41 as a function of pore size at 40 K. Solid line denotes the simulated pattern of the spheres of radius 1.4 nm with the structure of the low-temperature bulk α phase.

and amorphous patterns. We investigated the structure of the confined solid Kr by comparing the observed diffraction pattern with that simulated using the Debye formula appropriate to the calculation of the powder diffraction pattern of small particles.[31,32] The treatment was essentially the same as that used in the diffraction studies of rare gases confined in silica gel by Schafer et al.[25] The coordinates of the atoms in the simulated clusters were obtained by a successive stacking of close-packed layers. As Figure 10 shows, a good fit between the observed and calculated patterns was obtained with the incorporation of stacking faults, being consistent with the previous studies.[25] Here, the calculated spectrum (solid line) was obtained on spherical particles with a radius of 1.6 nm, a Kr−Kr distance of 0.4038 nm, and a 0.25 Å root-mean-square fluctuation (l_{ij}) of all the atoms. The intermolecular distance is consistent with that observed in the bulk phase.[33] This suggests that the solid Kr confined to the mesopores of MCM-41 consists of a mixture of crystalline structures intermediate between an fcc lattice and an hcp structure rather than the fcc lattice of the bulk phase. Neither pure phase of an fcc lattice or an hcp structure gave a good fit between the observed and calculated patterns. The present analysis neglects the interfacial phase confined between the microcrystal in the middle of the pores and the amorphous pore wall, as well as the cross-correlation term between molecules and silicas. Presumably these effects also contribute to the diffuse scattering component that is represented by the diffraction pattern for $R = 1.45$ nm.

Figure 11 shows the X-ray diffraction patterns of the frozen CO confined within MCM-41 as a function of pore size at 40 K. The diffraction patterns for $R = 2.9$ and 2.5 nm are crystalline, whereas that for $R = 2.1$ nm is amorphous. The diffraction pattern of the frozen CO within the cylindrical mesopores of $R = 2.9$ nm is compared with the simulated spectrum of spheres with the same structure as the low-temperature α phase, a lattice constant of 0.5686 nm, a nominal radius of 1.4 nm, and $l_{ij} = 0.20$ Å. The lattice constant is in a good agreement with that of the bulk.[34] Except for a diffuse background, all the features in the experimental diffraction pattern are well reproduced in simulation. This clearly indicates that on cooling the CO confined to the mesopores of MCM-41 solidifies directly into the orientationally ordered α phase without solidifying via the orientationally disordered β phase.

On the other hand, the N_2 confined within MCM-41 froze into an orientationally disordered solid with the structure similar to that of the high-temperature β phase. Figure 12 shows the X-ray diffraction patterns of the N_2 confined to the mesopores of MCM-41 as a function of pore size at 40 K. The diffraction patterns for $R = 2.9$ and 2.5 nm are crystalline, whereas that for $R = 2.1$ nm is amorphous. The diffraction pattern of the frozen N_2 confined to the mesopores of $R = 2.9$ nm is compared with the simulated spectrum of spheres with a nominal radius of 1.4 nm, the same intermolecular distance as that of the confined CO, and $l_{ij} = 0.20$ Å. Here, the simulated spectrum was obtained for a mixture of crystalline structures intermediate

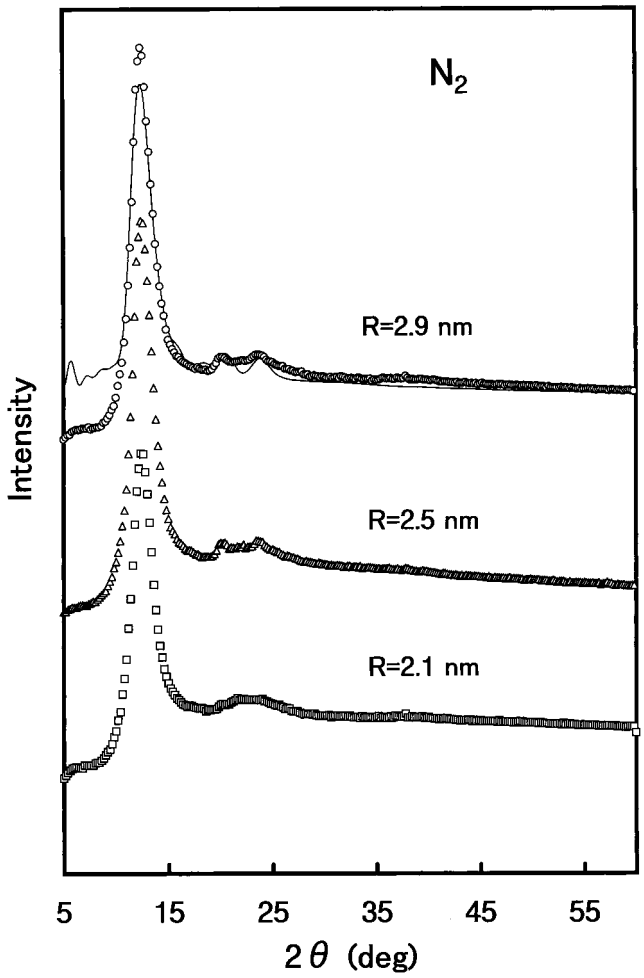

Figure 12. X-ray diffraction patterns of N_2 confined within MCM-41 as a function of pore size at 40 K. Solid line denotes the simulated pattern of the spheres of radius 1.4 nm with stacking sequence ABCBCABCA.

between an fcc lattice and an hcp structure with the same stacking faults as that of the confined Kr and with an orientational disorder. An hcp structure did not give a reasonable fit between the observed and calculated patterns, although the bulk β phase takes an hcp structure. All the features in the experimental diffraction pattern are well reproduced in simulation. The liquid N_2 confined to the mesopores of MCM-41 freezes into an orientationally disordered solid with packing sequence similar to that of the confined solid Kr.

The amount of the thermodynamical supercooling may be estimated according to the Gibbs−Thomson or related equation. A simple freezing model[7] for an idealized cylindrical pore of radius r predicts the liquids will solidify at an undercooling

$$\Delta T/T_o = 2\,\Delta\sigma v/(\Delta h_f r) \qquad (1)$$

where Δh_f is the enthalpy of fusion, T_o the bulk melting point, v the molar volume, and $\Delta\sigma$ the difference between the solid/wall interfacial energy and the liquid/wall interfacial energy. It is known that surface layers adjacent to the pore wall show freezing behavior different from that of the liquid in the center of the pores.[10,35,36] When the surface layer is still in a mobile state, the liquid in the central part of the pores freezes. Therefore, $\Delta\sigma$ may be taken as σ_{ls}, the liquid−solid interfacial free energy of the material. Equation 1 should also be valid in the case of the solid−solid transition, with the appropriate substitution of parameter. Unfortunately, as $\Delta\sigma$ for all these molecules is not known, we cannot estimate their freezing point depressions. Figure 13 shows the pore-size dependence of the freezing points for N_2, CO, and Kr confined within MCM-41, together with that for H_2O[12] confined within MCM-41. The freezing-point depressions of the CO and N_2, normalized to T_o, are nearly the same and are slightly larger than that of the Kr. Freezing of the CO confined to the mesopores resulted in the appearance of the orientationally ordered α phase, whereas the N_2 solidified into the orientationally disordered phase analogous to the bulk β phase. Such a difference seems to depend on whether the stable phase at the freezing point is the orientationally disordered phase or the orientationally ordered phase. The freezing points of the CO are situated well below the α−β transition point, whereas those of the N_2 are situated within the wide stability region of the bulk β phase. As T_o of the liquid−α phase transition is not known, T_o of the liquid−β phase transition was also used in the calculation of $\Delta T/T_o$ for the CO.

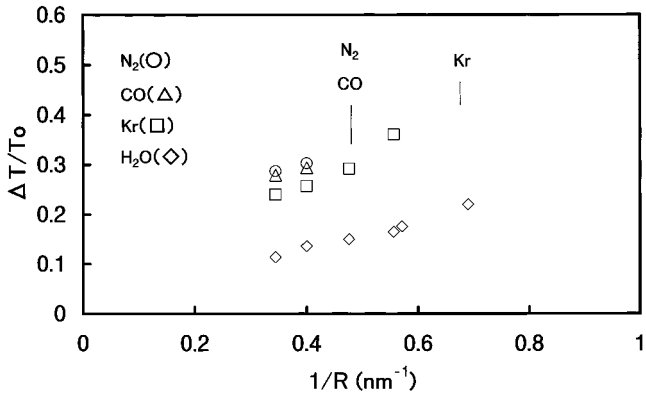

Figure 13. Freezing-point depressions as a function of $1/R$ for N_2, CO, Kr, and H_2O confined within MCM-41. Vertical lines denote the maximum pore size, below which upon cooling vitrification of confined liquids occurs within the cylindrical mesopores.

B. Vitrification of pore liquids. Vitrification of liquids confined to the small pores upon cooling has been reported for many systems.[4,6,8,13,18,25,37] Some researchers[4,25] have thought that the interactions between the liquids and the amorphous pore wall play an important role in the appearance of the glassy state. This is in contradiction with the results of recent studies[38−41] concerning dynamics of liquids confined in porous silicas. All these studies indicate that the surface-bound layer, with dynamic properties different from that of the liquid in the center of the pores, is limited within the first one or two layers adjacent to pore wall, irrespective of the kind of liquids. These surface layers are presumably frozen into an amorphous structure to accommodate the complex wall geometry, at lower temperatures than expected from the Gibbs−Thomson effect for the liquids in the center of the pores.

As Figure 13 shows, the maximum pore size below which vitrification of a liquid confined within the cylindrical mesopores upon cooling occurs depends on the molecules. On freezing, the N_2 and CO confined to the cylindrical mesopores of R = 2.1 nm vitrify, whereas the Kr confined to the mesopores of R = 2.1 and 1.8 nm crystallizes. A confined Kr phase vitrifies within the mesopores of R = 1.45 nm. On the other hand, water crystallizes even in the small mesopores of R = 1.2 nm. The freezing-point depressions of a confined water due to the Gibbs−Thomson effect are small compared with the glass transition temperature (T_g), $(T_o - T_g)/T_o = 0.502$.[42] Therefore, a confined water, except for the bound water adjacent to the pore wall, must crystallize in the course of freezing. The freezing-point depressions, normalized to the bulk melting point, for liquids N_2, CO, and Kr are more than twice that for water.

$\Delta T/T_o$ for these simple molecules attains 0.3−0.4 in the smallest pores where freezing can result in crystallization. An empirical rule that connects the glass transition temperature to the melting point, viz. the $T_g/T_o \approx 2/3$ rule,[43] suggests that such deep supercooling may lead to vitrification of these molecular liquids confined to the mesopores.

References and Notes

(1) Sullivan, N. S.; Rall, M.; Brison, J. P. *J. Low Temp. Phys*. **1995**, *98*, 383.
(2) Molz, E.; Wong, A. P. Y.; Chan, M. H. W.; Beamish, J. R. *Phys. Rev. B* **1993**, *48*, 5741.
(3) Wang, Y.; Snow, W. M.; Sokol, P. E. *J. Low Temp. Phys*. **1995**, *101*, 929.
(4) Sokol, P. E.; Ma, W. J.; Herwig, K. W.; Snow, W. M.; Wang, Y.; Koplik, J.; Banavar, J. R. *Appl. Phys. Lett*. **1992**, *61*, 777.
(5) Bittner, D. N.; Adams, E. D. *J. Low Temp. Phys*. **1994**, *97*, 519.
(6) Coulomb, J. P.; Martin, C.; Grillet, Y.; Llewellyn, P. L.; Andre, G. In *Mesoporous Molecular Sieves*; Bonneviot, L., Beland, F., Danumah, C., Giasson, S., Kaleaguine, S., Eds.; Studies in Surface Science and Catalysis 117; Elsevier: Amsterdam, 1998; p 309.
(7) Awschalom, D. D.; Warnock, J. *Phys. Rev. B* **1987**, *35*, 6779.
(8) Llewellyn, P. L.; Grillet, Y.; Rouquerol, J.; Martin, C.; Coulomb, J.-P. *Surf. Sci*. **1996**, *352*−*354*, 468.
(9) Brown, D. W.; Sokol, P. E.; Clarke, A. P.; Alam, M. A.; Nuttall, W. J. *J. Phys. Condens. Matter* **1997**, *9*, 7317.
(10) Schmidt, R.; Hansen, E. W.; Slocker, M.; Akporiaye, D.; Ellestad, O. H. *J. Am. Chem. Soc*. **1995**, *117*, 4049.
(11) Takamuku, T.; Yamagami, M.; Wakita, H.; Masuda, Y.; Yamaguchi, T. *J. Phys. Chem. B* **1997**, *101*, 5730.
(12) Morishige, K.; Kawano, K. *J. Chem. Phys*. **1999**, *110*, 4867.
(13) Morishige, K.; Kawano, K. *J. Phys. Chem. B* **1999**, *103*, 7906.
(14) Mu, R.; Malhotra, V. M. *Phys. Rev. B* **1992**, *46*, 532.
(15) Booth, H. F.; Strange, J. H. *Mol. Phys*. **1998**, *93*, 263.
(16) Grosse, K.; Ratke, L.; Feuerbacher, B. *Phys. Rev. B* **1997**, *55*, 2894.
(17) Mu, R.; Xue, Y.; Henderson, D. O.; Frazier, D. O. *Phys. Rev. B* **1996**, *53*, 6041.
(18) Mu, R.; Jin, F.; Morgan, S. H.; Henderson, D. O.; Silberman, E. *J. Chem. Phys*. **1994**, *100*, 7749.
(19) Unruh, K. M.; Huber, T. E.; Huber, C. A. *Phys. Rev. B* **1993**, *48*, 9021.
(20) Charnaya, E. V.; Tien, C.; Lin, K. J.; Kumzerov, Y. A. *Phys. Rev. B* **1998**, *58*, 11089.
(21) Kumzerov, Y. A.; Nabereznov, A. A.; Vakhrushev, S. B.; Savenko, B. N. *Phys. Rev. B* **1995**, *52*, 4772.
(22) Borisov, B. F.; Charnaya, E. V.; Plotnikov, P. G.; Hoffmann, W.-D.; Michel, D.; Kumzerov, Y. A.; Tien, C.; Wur, C.-S. *Phys. Rev. B* **1998**, *58*, 5329.
(23) Kresge, C. T.; Leonowicz, M. E.; Roth, W. J.; Vartuli, J. C.; Beck, J. S. *Nature (London)* **1992**, *359*, 710.
(24) Morishige, K.; Shikimi, M. *J. Chem. Phys*. **1998**, *108*, 7821.
(25) Schafer, B.; Balszunat, D.; Langel, W.; Asmussen, B. *Mol. Phys*. **1996**, *89*, 1057.
(26) Scott, T. A. *Phys. Rept*. **1976**, *27C*, 89.
(27) Hall, B. O.; James, H. M. *Phys. Rev. B* **1976**, *13*, 3590.
(28) Morishige, K.; Inoue, K.; Imai, K. *Langmuir* **1996**, *12*, 4889.
(29) *Kagakubinran-kisohen II*; The Chemical Society of Japan, Eds.; Maruzen: Tokyo, 1993; p 243.
(30) You, H.; Fain, Jr., S. C. *Surf. Sci*. **1985**, *151*, 361.
(31) Morozumi, C.; Ritter, M. L. *Acta Crystallogr*. **1953**, *6*, 588.
(32) Bawendi, M. G.; Kortan, A. R.; Steigerwald, M. L.; Brus, L. E. *J. Chem. Phys*. **1989**, *91*, 7282.
(33) Pollack, G. L. *Rev. Mod. Phys*. **1964**, *36*, 748.
(34) Krupskii, I. N.; Prokhvatilov, A. I.; Erenburg, A. I.; Yantsevich, L. D. *Phys. Status Solidi A* **1973**, *19*, 519.
(35) Pearson, R. T.; Derbyshire, W. *J. Colloid Interface Sci*. **1974**, *46*, 232.
(36) Overloop, K.; van Gerven, L. *J. Magn. Reson., Ser. A* **1993**, *101*, 179.
(37) Booth, H. F.; Strange, J. H. *Mol. Phys*. **1998**, *93*, 263.
(38) Staph, S.; Kimmich, R. *J. Chem. Phys*. **1995**, *103*, 2247.
(39) Zavada, T.; Kimmich, R. *J. Chem. Phys*. **1998**, *109*, 6929.
(40) Loughnane, B. J.; Fourkas, J. T. *J. Phys. Chem. B* **1998**, *102*, 10288.
(41) Loughnane, B. J.; Scodinu, A.; Fourkas, J. T. *J. Phys. Chem. B* **1999**, *103*, 6061.
(42) Speedy, R. J. *J. Phys. Chem. B* **1999**, *103*, 4060.
(43) Alba-Simionesco, C.; Fan, J.; Angell, C. A. *J. Chem. Phys*. **1999**, *110*, 5262.